

# Caustics of finitely dense inertial particles

C. Rajarshi  <sup>1,\*</sup> and Rama Govindarajan  <sup>1,†</sup>

<sup>1</sup>*International Centre for Theoretical Sciences,  
Tata Institute of Fundamental Research, Bangalore 560089, India*

Estimating collision rates is of immense importance in particle-laden flows. An economical way of doing this is to directly identify incidences of caustics, or extreme clustering, by tracking particle velocity gradients in the neighborhoods of individual particles. The objective of this work is two-fold. (i) We find conditions under which caustics form, in point-vortex flow and in two-dimensional turbulence. While caustics are known to form in regions of strain, we show that the velocity alignment with strain directions is key. Particles must remain in compressional strain throughout the process to form caustics, whereas survivor particles: which visit high strain but do not form caustics, briefly go through extensional strain during the early part of the process. This enables survivor particles to attain significantly straighter paths, and to move faster, whereas caustics particles follow paths of high curvature and move slower. As a result, caustics particles stay longer in high-strain regions than survivors. (ii) We ask about the effect of finite particle density, where the particle is denser than the background fluid. We show that finite-density particles need to sample stronger background strain than infinite-density ones to trigger caustics, but our other findings are universal across particle density.

## I. INTRODUCTION

Pollens that spread forests, pollutants that smother cities, water droplets that rain, and oceanic plankton that control the global carbon cycle are all particles suspended in, and heavily dominated by, a turbulent background flow. Such particles are often denser than the background fluid and are of finite size. They thus have non-zero inertia and respond to turbulence by centrifuging out of vortical regions, accumulating in high-strain regions. This phenomenon is called preferential clustering [1–3]. Particles undergoing extreme clustering collide with each other, forming caustics. During caustics, particles distributed initially in two or three dimensions come so close together that they may occupy a smaller spatial dimension. These collisions or caustics are central to rain formation [4–7], planetesimal formation in protoplanetary disks [8–11], and for maintaining populations of small creatures in the ocean by enhancing reproduction rates.

Though rare in dilute suspensions, caustics are thus crucial for our very survival. The mechanism of how turbulence promotes caustics is not entirely clear, and this paper deals with one aspect: we ask how high a strain a finitely dense caustics particle needs to experience, and what makes other particles that do experience such strain not form caustics. The situations of our interest involve  $O(10^j)$  particles, where  $j$  is far too large for numerical solutions of individual particle dynamics to be feasible. One may resort to continuum descriptions where the particles are described by a compressible velocity field  $\mathbf{v}(t, \mathbf{x})$  on the space  $\mathbf{x}$ . Caustics are singular points of extreme compression of this field, where the rate of change of the particle number density diverges at finite time, i.e.,  $\nabla \cdot \mathbf{v} \rightarrow -\infty$  [4]. These can be identified by evolving the dynamics of representative particles as well as particle velocity gradients at each particle's location, directly in a Lagrangian sense. This captures the behavior of an infinitesimal particle parcel in its neighborhood [4, 12].

\* [rajarshic.edu@gmail.com](mailto:rajarshic.edu@gmail.com)

† [rama@icts.res.in](mailto:rama@icts.res.in)

With this approach, we may characterize caustics formation in a turbulence field by following a relatively small number of particles.

Caustics have been identified [4–6] as a potential mechanism for abrupt droplet growth causing rain showers. Falkovich and Pumir [13] found collision rates in cloud droplets due to caustics to be higher than previous geometric arguments. Later Bhatnagar *et al.* [14] looked for, but did not find, a scaling for the rate of caustics formation of infinitely dense particles as a function of particle size or its Stokes number. Modeling the fluid velocity gradient as white noise, Barta and Vollmer [15] found that there are infinite ways to form caustics in the phase space of invariants of the particle velocity gradient tensor. We note, however, that velocity gradients in turbulence are highly non-Gaussian [16]. Studying collisions between individual infinitely-dense particles, Picardo *et al.* [17] showed that high-strain regions, just outside vortices, facilitate head-on collisions.

The present study builds on two others. The first is the work of Meibohm *et al.* [12], who derive a caustics condition, expressed as an inequality, in two-dimensional flow for small infinitely-dense particles, and subsequently [18] a condition in three-dimensional flow. As we discuss later, these conditions are derived for particles ‘frozen’ in place. Direct numerical simulations (DNS) [19], showed that caustics events do not always satisfy these inequalities. The second is that of Bätge *et al.* [20], who found the inequality to not be a sufficient condition for infinitely-dense particle caustics, and assuming that the fluid and the particle gradient matrices commute with each other during caustics, showed analytically that particles need to remain within regions of extreme strain for long enough times in order to undergo caustics. They further confirmed this through direct numerical simulations.

While caustics are known to form in strain regions, we ask what kind of strain and how it affects the outcome. Secondly, all real particles are finitely dense, and their caustics formation has not been studied, to our knowledge. We do so in two-dimensional flows for particles denser than the fluid. We extend the Lagrangian equation for detecting caustics to finite density particles in the §II, and discuss its advantages. Next in §III, we follow [12, 18] to study caustics formation of artificially frozen particles, since it is analytically appealing and reveals some general features. Thereafter, we study caustics formation of particles moving as they should, in two flows: a toy flow in §IV A consisting of a single point-vortex, and two-dimensional turbulence in §IV B. Lastly, in §V, we summarize our findings and discuss their implications.

## II. SETTING UP OF THE PROBLEM

We assume one-way coupling, i.e., that particles are too small to affect the flow and are in dilute enough suspension so as not to influence each other. In the limit of negligible Reynolds number, a spherical particle of velocity  $\mathbf{v}(t)$  and position  $\mathbf{x}_p(t)$  at time  $t$  obeys the Gatignol-Maxey-Riley equation[21, 22], which, in its simplest form, reads, in non-dimensional terms, as

$$\frac{d\mathbf{x}_p}{dt} = \mathbf{v} \quad ; \quad \frac{d\mathbf{v}}{dt} = \frac{\alpha}{St} (\mathbf{u} - \mathbf{v}) + 3(1 - \alpha) \frac{D\mathbf{u}}{Dt}, \quad (1)$$

where  $\mathbf{u} = \mathbf{u}(t, \mathbf{x}_p(t))$  is the velocity of the background fluid at the particle’s position. We have ignored the effects of external forces such as gravity on the particles, and used characteristic flow length and velocity scales  $L$ , and  $L/\tau_f$  respectively, where  $\tau_f$  is the evolution timescale of the background fluid. The nondimensional parameters in the problem are the density ratio  $\rho \equiv \rho_p/\rho_f$ , appearing in terms of the density parameter  $\alpha \equiv 2\rho/(2\rho + 1)$ , and the Stokes number  $St \equiv \tau_p/\tau_f$  where  $\tau_p = 2a^2\rho/(9\nu)$ . The subscripts  $p$  and  $f$  stand for particle and fluid, respectively,  $a$  is a

particle's radius, and  $\nu$  the kinematic viscosity of the fluid. We are interested in particles denser than the fluid, with  $2/3 < \alpha \leq 1$ , where  $2/3$  corresponds to neutrally buoyant particles and  $1$  to infinitely-dense particles. We note that when  $\alpha = 1$ ,  $\mathbf{v} = \mathbf{u}$  is a solution of Eq. (1), whereas this is not the case for finitely-dense particles. Added mass and fluid acceleration make up the last term in Eq. (1), which are absent in the dynamics of an infinitely-dense particle. Due to these additional forces, centrifugation by vortices, as well as clustering rates in strain regions are weaker at lower particle densities [2, 3, 23–28]. This hints at a lower formation rate of caustics for finitely dense particles. Eq. (1) ignores the finite size, lift, and Basset-Boussinesq history effects on the particle. Finite size decreases acceleration fluctuations, as seen for neutrally buoyant particles [29], and ignoring them restricts us to small particle sizes. Lift forces, proportional to the vorticity the particles experience [30], govern the dynamics of bubbles [31] but are relatively weak for particles denser than the fluid as they centrifuge out of vortices and live in strain regions. History forces affect clustering at  $O(1)$  Stokes number [32, 33]. Practical situations concerning caustics and collisions involve small  $St$  particles, where Ferry and Balachandar [34] showed that the history force is less important than the added mass. Our recent work [35] shows that history effects are quantitative rather than qualitative in the sense that particles of large Stokes number with history forces included behaved like those at smaller Stokes number where history was neglected. Still, whether neglecting Basset-Boussinesq history is justified will be a factor for future evaluation. Given the heavy computational load it entails, it is common to neglect it in early studies of a phenomenon, as we do here. We believe that the physics we uncover will hold with history effects as well.

Eq. (1), with  $d/dt \equiv \partial/\partial t + \mathbf{v} \cdot \nabla$ , applies to a continuum of particles, under the assumption that  $\mathbf{v}$  is continuous in space. The particle continuity equation reads

$$\frac{dn}{dt} = -n \nabla \cdot \mathbf{v}. \quad (2)$$

We see that at caustics, when  $\nabla \cdot \mathbf{v} \rightarrow -\infty$ , the particle number density  $n$  also diverges. In terms of the particle velocity gradient matrix  $\mathbb{Z} \equiv St \nabla \mathbf{v}$  [4, 12], caustics happen when  $\text{Tr}(\mathbb{Z}) \rightarrow -\infty$ . From Eq. (1), we can show that for finitely-dense particles,  $\mathbb{Z}$  is related to the fluid velocity gradient matrix  $\mathbb{A} = St \nabla \mathbf{u}$  by

$$\frac{d\mathbb{Z}}{dt} = -\frac{\alpha}{St} (\mathbb{Z} - \mathbb{A}) - \frac{1}{St} \mathbb{Z}^2 + 3(1-\alpha) \left[ \frac{D\mathbb{A}}{Dt} + \frac{1}{St} \mathbb{A}^2 \right]. \quad (3)$$

In the limit of infinite particle density, i.e.,  $\alpha = 1$ , the above equation reduces to

$$St \frac{d\mathbb{Z}}{dt} = \mathbb{A} - \mathbb{Z} - \mathbb{Z}^2, \quad (4)$$

which has appeared before in the literature (see e.g. [4, 6, 18]). For tracking of caustics, Eq. (3) presents us with tremendous advantages over both solving for individual particles using Eq. (1) and solving for a continuous  $\mathbf{v}$  field on Eulerian grid points. To obtain reliable statistics out of chance collisions between particle pairs, a numerical approach would need a prohibitively large number of particles. On the other hand, once a single collision occurs in an Eulerian grid, i.e.,  $-\nabla \cdot \mathbf{v}$  diverges somewhere in the domain, the simulation cannot be continued, and there is no future after caustics. In the present approach we seed the flow with a finite number of particles and solve for the particle dynamics using Eq. (1), alongside solving for the particle velocity gradient tensor  $\mathbb{Z}$  using Eq. (3). The singularities now remain restricted to individual particles, and can be artificially removed [13]. A noteworthy limitation of this approach is that it cannot capture collisions of faraway particles approaching each other at high speed.

In the limit  $St \rightarrow 0$ ,  $\mathbf{v} \rightarrow \mathbf{u}$  by Eq. (1), but by Eq. (3),  $\mathbb{Z}$  does not relax to  $\mathbb{A}$ . Thus, clusters once formed cannot be unclustered with ease by the background flow. Also, if the magnitude of the

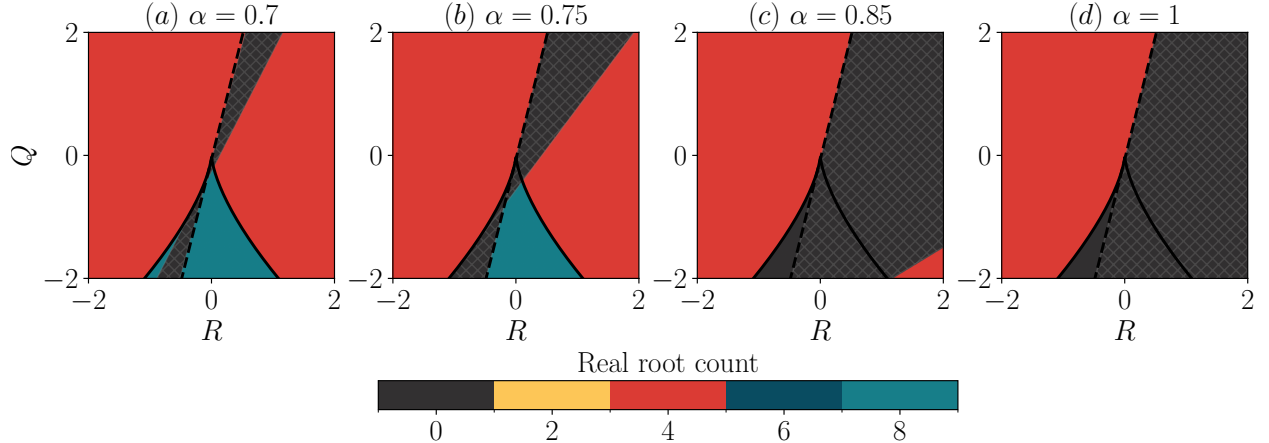


FIG. 1: Number of real roots of Eq. (7) in the  $QR$  plane. The hatched area satisfies Eq. (6), which is a sufficient condition for caustics, while there are some regions with zero roots even outside it. The solid black line is the Vieillefosse line following  $Q^3 + 27/4R^2 = 0$  (see [36] for details). The black dashed lines show  $Q - 4R = -1/16$ , the caustics condition for  $\alpha = 1$ .

entries of  $\mathbb{Z}$  become large enough that  $-\mathbb{Z}^2$  eclipses all other terms on the right-hand side of Eq. (3), caustics become inevitable. Denoting such a state by  $\mathbb{Z} = \mathbb{Z}_b$  at time  $t = t_b$ , caustics occur in finite time  $(t - t_b) \sim St/\mathbb{Z}_c$ . This hints at a universality in caustics formation for particles of any density.

### III. CAUSTICS ON “FROZEN” PARTICLES

Setting  $\mathbb{A}$  to a constant in Eq. (3) has the effect of ‘freezing’ the particles in place in a steady flow, while allowing for local clustering, denoted by  $\mathbb{Z}$ , to evolve. This is an artificial but useful construct, since it enables analytical reduction. And, a moving particle that spends a lot of time within a frozen-particle-caustics-region has a higher chance of attaining caustics. Meibohm *et al.* [12, 18] froze their  $\alpha = 1$  particles (without explicitly mentioning this), and showed that the system in Eq. (4) has two options. If a real  $\mathbb{Z} = \mathbb{Z}_0$  satisfies Eq. (4) the system may attain this fixed point. If no such  $\mathbb{Z}_0$  exists, and  $St \rightarrow 0$ , caustics inevitably result. Caustics occur whenever  $Q - 4R < -1/16$  where  $Q = -\text{Tr}(\mathbb{A}^2)/2$  and  $R = -\det(\mathbb{A})$ . In two dimensions (2D),  $R = 0$ , and this reduces to  $Q < -1/16$ . Note that  $Q$  is the Okubo-Weiss parameter that indicates how vortical ( $Q > 0$ ) or strain ( $Q < 0$ ) dominated a given point in the flow is. We shall see that particles visiting high negative values of  $Q$ , i.e., high-strain regions, is essential to caustics formation. Following [12], we derive a caustics condition for finitely-dense frozen particles with  $St \rightarrow 0$ :

$$-\alpha(\mathbb{Z} - \mathbb{A}) - \mathbb{Z}^2 + 3(1 - \alpha)\mathbb{A}^2 \neq 0. \quad (5)$$

As derived in Appendix A, and defining  $\xi \equiv 1 - \alpha$ , regions of the background flow satisfying

$$\alpha^2 \left[ \alpha^4 + 144\xi^2 Q^2 + 8(3\alpha - 1)\alpha^2 Q \right] - 16\alpha R \left[ \alpha^2(9\alpha - 5) + 36\xi^2 Q \right] + 1728\xi^3 R^2 < 0 \quad (6)$$

satisfy the inequality (5) for any real  $\mathbb{Z}$ , resulting in frozen-particle caustics. For  $\alpha = 1$ , Eq. (6) reduces to the linear relationship of [18]. The gray regions with crossed white hatches regions in Fig. 1 satisfy Eq. (6), whereas solid colors correspond to different numbers of real roots of

$$-\alpha(\mathbb{Z} - \mathbb{A}) - \mathbb{Z}^2 + 3(1 - \alpha)\mathbb{A}^2 = 0, \quad (7)$$

where caustics may not occur. In these regions, we find that there is at least one stable root (not shown). We note that Eq. (6) presents a sufficient condition for caustics, and that there can be regions outside it too with zero roots, as seen in Fig. 1, and where caustics can therefore occur. Defining  $\delta \equiv \text{Tr}(\mathbb{Z}) = St\nabla \cdot \mathbf{v}$  and taking the trace of Eq. (3), we get

$$St \frac{d\delta}{dt} = -\alpha\delta - \text{Tr}(\mathbb{Z}^2) - 6(1-\alpha)Q. \quad (8)$$

We see that for finitely-dense particles, a large negative  $Q$  makes a positive contribution to  $\delta$ , taking it away from caustics. This is remarkable, because high strain is normally expected to be positively correlated with caustics formation. So finite-density particles contain physics competing with the standard clustering effect of strain.

#### IV. CAUSTICS IN TWO-DIMENSIONAL FLOWS

##### A. Point Vortex Flow

Before moving to 2D turbulence, it is insightful to study caustics in the vicinity of a point vortex. The dimensional velocity field is given by  $\mathbf{u}^* = \hat{\theta} \Gamma / 2\pi r^*$ , where  $r^*$  is the dimensional length from the origin, and  $\Gamma$  is the circulation. Choosing the length scale  $L = \sqrt{\Gamma\tau_p/2\pi}$  [37] and timescale  $\tau_p$ , the nondimensional velocity and the invariant  $Q$  become

$$\mathbf{u} = \frac{1}{r} \hat{\theta}, \quad \text{and} \quad Q = -\frac{1}{r^4}, \quad (9)$$

whereas the invariant  $R = 0$  because this is a 2D flow. The entire flow is thus in a strain field which is singular at the point vortex and rapidly decays away from it. Using Eq. (1), the non-dimensional equation of motion of particles around a point vortex in polar coordinates  $\mathbf{x}_p = (r, \theta)$  reads

$$\ddot{r} + \alpha\dot{r} = \frac{\mathcal{L}^2 - 3(1-\alpha)}{r^3} \quad ; \quad \dot{\mathcal{L}} = \alpha(1-\mathcal{L}), \quad (10)$$

which is an extension to  $\alpha \neq 1$  of the expression of [37], and where  $\mathcal{L} = r^2\dot{\theta}$  is the angular momentum per unit mass, and  $\dot{(\cdot)} = d(\cdot)/dt$ . Our choice of scales renders Eq. (10) parameter-free, so a given solution holds for particles of any Stokes number when appropriately scaled. We show results for  $St = 1$ .

Eq. (10) may be solved for  $\mathcal{L}$  to give  $\mathcal{L}(t) = 1 - (1 - \mathcal{L}(0))e^{-\alpha t}$ . In fact, if we start from  $\mathbf{v}(0) = \mathbf{u}(r(0))$ , we have  $\mathcal{L} = 1$  for all time. Caustics happen when two rings of particles at different initial radii cross each other. Due to the circular symmetry of the system, we need to evolve just one particle for each ring. Infinitely-dense particles lying within a threshold radius from the point vortex all form caustics [38], while those beyond never do. The threshold, however, is only significant in real turbulence where the vorticity is comparable to or greater than the particle's relaxation rate [39]. Ravichandran and Govindarajan [37] recognized that the early-time dynamics of particles lying close to the vortex, i.e., in higher strain regions, determine their caustics formation. In other words, caustics is governed by the inner solution in a singular value problem, for which we define the inner variables  $\mathcal{R} = r/\ell$  and  $T = t/\tau$ , with  $\tau, \ell \ll 1$ . We follow the usual procedure in singular perturbation problems: of expanding the inner variables in powers of the small parameter  $\tau$ , and deriving the lowest order equation. The scaling of  $l \sim \sqrt{\tau}$  [40] yields physical solutions, and our choice of  $\ell^2 = \tau\sqrt{3\alpha - 2}$  yields the following parameter-free equation, valid for all Stokes numbers and all particle densities at the lowest order:

$$\mathcal{R}'' = \mathcal{R}^{-3}, \quad \text{whose solution is} \quad \mathcal{R}(T) = \sqrt{\frac{T^2}{\mathcal{R}_0^2} + \mathcal{R}_0^2}, \quad (11)$$

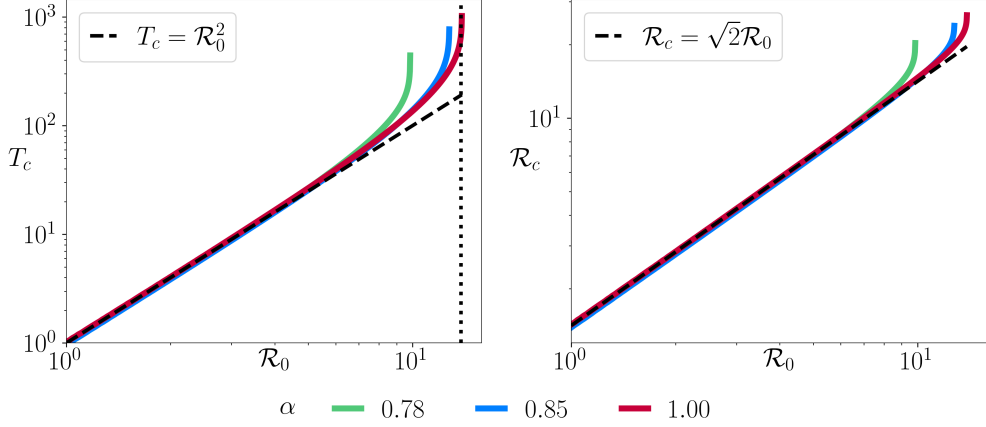


FIG. 2: Caustics time (a) and radius (b) in point-vortex flow as a function of the initial radial location, for particles of different density and of any Stokes number. The dashed line shows the inner solutions  $T_c = R_0^2$ , and  $R_c = \sqrt{2}R_0$ . In this scaling, caustics formation in the inner region is independent of particle density. The vertical dotted line indicates the location at which caustics time diverges for  $\alpha = 1$ , and beyond which caustics are not possible.

where  $(\cdot)' = d(\cdot)/dT$ , and  $\mathcal{R}_0 = \mathcal{R}(0)$ . This inner solution is valid close to the vortex origin and always yields caustics. Two rings with initial radius  $\mathcal{R}_0$  and  $\mathcal{R}_0 + \epsilon$  will form caustics at time  $T_c$ , given by

$$\sqrt{\frac{T_c^2}{\mathcal{R}_0^2} + \mathcal{R}_0^2} = \sqrt{\frac{T_c^2}{(\mathcal{R}_0 + \epsilon)^2} + (\mathcal{R}_0 + \epsilon)^2} . \quad (12)$$

In the limit  $\epsilon \rightarrow 0$ , a Taylor expansion yields  $T_c = \mathcal{R}_0^2$  and the caustics radius  $\mathcal{R}_c = \mathcal{R}(T_c) = \sqrt{2}\mathcal{R}_0$ . In the original variables of  $t = \tau T$  and  $r = \ell\mathcal{R}$ , the caustics radius and time read

$$r_c = \sqrt{2}r_0 \quad ; \quad t_c = \frac{r_0^2}{\sqrt{3\alpha - 2}} . \quad (13)$$

This immediately tells us that the caustics time scales as  $(3\alpha - 2)^{-1/2}$ , and diverges for neutrally buoyant ( $\alpha = 2/3$ ) particles, ensuring no caustics for them. And the size  $\ell$  of the inner region, which is proportional to  $r_c$ , scales as  $(3\alpha - 2)^{1/4}$ , shrinking to 0 for neutrally buoyant particles. The scaled caustics radius ( $\mathcal{R}_c$ ) and time ( $T_c$ ) obtained from numerical simulations of the complete equation Eq. (10) are shown in colors in Fig. 2(a,b) respectively. We see that the analytically obtained solution (black dashed lines) matches well with the numerical results close to the vortex origin. When  $\mathcal{R}_0 \gg 1$ , the inner solution is no longer valid, and the numerical solution differs from it. Importantly, the caustics time diverges beyond a critical initial radius  $\mathcal{R}_{c0}$  for each  $\alpha$ . Particles of any density beginning life within their respective  $\mathcal{R}_{c0}$  always form caustics. We call them ‘C’ particles. In contrast, all those starting out further away from the vortex never experience high strain and avoid caustics. Accordingly, we call them ‘avoiders’ or ‘A’ particles.

We may also identify the region for frozen-particle caustics by solving for  $r$  in Eq. (6):

$$\left[4(3\alpha - 1) - 8\sqrt{3\alpha - 2}\right]^{\frac{1}{4}} < r\sqrt{\alpha} < \left[4(3\alpha - 1) + 8\sqrt{3\alpha - 2}\right]^{\frac{1}{4}} . \quad (14)$$

This result is very different from our moving particle analysis. The reason for this major discrepancy is that Eq. (14) assumes that a particle that is initially within the region described by Eq. (14)

stays within it until caustics form. Moving particles that escape this region in time shorter than  $St$  escape caustics even though they started life in a conducive region for frozen-particle caustics.

## B. Two-dimensional turbulence

Armed with the insights from point-vortex flow, we investigate caustics of finitely-dense particles in steady state two-dimensional turbulence, by evolving an incompressible turbulent flow field  $\mathbf{u} = (u_x, u_y)$  with vorticity  $\omega = \partial_x u_y - \partial_y u_x$ , which is evolved according to

$$\partial_t \omega + \mathbf{u} \cdot \nabla \omega = \nu \nabla^2 \omega - \gamma \omega + f_\omega. \quad (15)$$

A small linear drag with coefficient  $\gamma$  (here set at  $10^{-2}$ ) is added to prevent a numerical blow-up caused by the inverse energy cascade in 2D turbulence. Following [41], we set the external forcing function  $f_\omega = -\nu k_f (\cos(k_f x) + \sin(k_f x))$ , where  $k_f = 4$  is the forcing wavenumber. The initial vorticity is  $\omega(0) = k_f \cos(k_f x)$ , and the viscosity  $\nu = 8 \times 10^{-6}$ . We evolve the flow using a pseudospectral simulation on a  $1024 \times 1024$  grid with doubly periodic boundary conditions, and a fourth-order Runge-Kutta time-stepping. At the steady state, the Kolmogorov time is  $\tau_f = 4.0$  in simulation units.  $3.14 \times 10^5$  inertial particles of  $St=0.225$ , unless otherwise specified, that obey Eq. (1) are inserted randomly across the flow once the turbulence has reached a stationary state. At this initial time,  $\mathbf{v}$  and  $\mathbb{Z}$  of each particle are set equal to  $\mathbf{u}$  and  $\mathbb{A}$ , respectively, interpolated to its position. We use sixth-order B-spline interpolation [42], and  $\mathbb{Z}$  is evolved according to Eq. (3). When  $\delta = \text{Tr}(\mathbb{Z})$  crosses  $-20$  for any particle, it is taken to have undergone caustics, as caustics are found to be inevitable thereafter. Beyond caustics, to keep particle number constant, we reinitialize the particle by setting  $\mathbb{Z} \rightarrow -\mathbb{Z}$ . This transformation is equivalent to the infinitesimal particle volume element reemerging after caustics as ghost particles [13] occupying a small finite volume. Simulations for different  $\alpha$  are run up to a time of  $125\tau_\eta$ , and statistics are collected over this time.

Figure 3 shows the vorticity snapshot of the background flow with inertial particles overlaid, for  $\alpha = 0.7, 0.77$  and  $1.0$ . Denser particles centrifuge out of vortices more readily than their lighter counterparts, as in previous studies [2, 3, 25–28, 43], since lighter particles’ centrifugation is hindered by their added mass [2]. Denser particles show higher clustering levels in strain regions. C particles (in cyan), increase in number with increasing particle density, and live alongside other particles in the strain region. Fig. 3(d) compares the distribution of  $Q$  in the background field to those sampled by *all* particles. As we know, extreme vortices are more common than extreme strain in 2D turbulence. The inset of Fig. 3(d) shows that the mean  $Q$  experienced by particles is a small negative number for particles, whereas this quantity is zero for the background flow. Interestingly, the leftmost part of Fig. 3(d) shows that denser particles are infrequent in visiting regions of extreme strain as compared to their lower-density counterparts. We think this is because high strain is associated with rapid acceleration and deceleration in the flow, and high-density particles are less able to adapt to these changes due to their inertia.

### 1. Behavior of caustics or C particles

In Fig. 4 (a-c) we show that C particles of all densities undergo a particular history of the  $Q$  field immediately before the caustics formation time  $t_c$ , experiencing a maximum in strain or minimum  $Q$  at  $t = t_m$ , which is  $5 - 8$  time units before  $t_c$ . Each particle’s time-series has been shifted so that their  $t_c$ ’s coincide. The dashed lines show the mean of the PDFs at each time, and its minimum is denoted by  $\langle Q \rangle_{min}$ . Fig. 4(g) shows  $\langle Q \rangle_{min}$  against  $\alpha$  for two Stokes numbers. Lower density particles have lower  $\langle Q \rangle_{min}$ , indicating that they need to go through regions of more intense strain

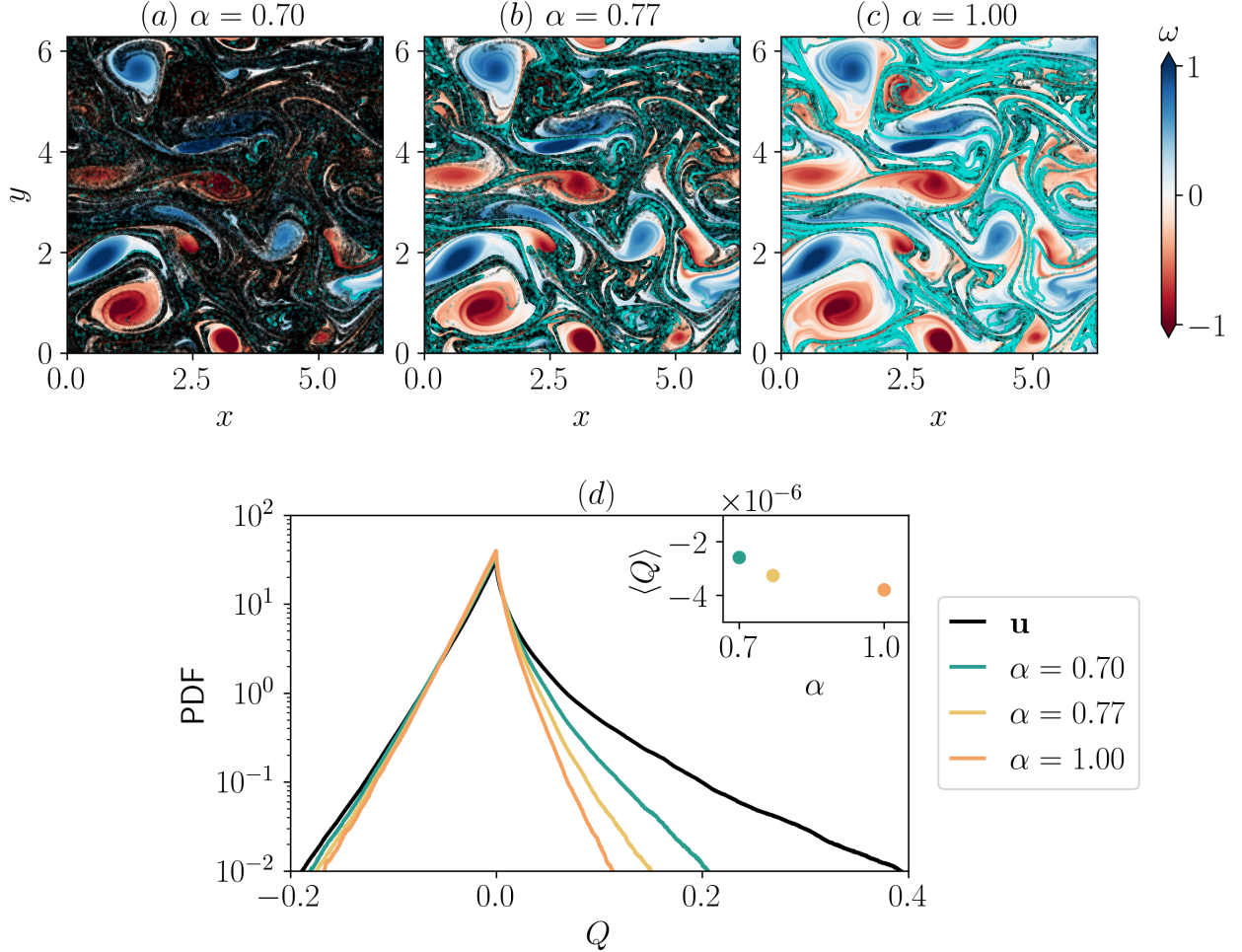


FIG. 3: (a-c) Snapshots of the vorticity field  $\omega$  overlaid with caustics C particles in cyan, and the remaining ones in black at  $t = 333 St$ . All particles centrifuge out of large vortices and live in strain regions. As expected from prior studies [2, 3, 25–28], lowering the particle density weakens centrifugation. (d) PDF of the time-averaged  $Q$  experienced by the particles (in color), as well as that of the background field (in black). Progressive emptying of high vorticity regions with increasing particle density is seen.

than their denser counterparts to form caustics. This is also true in point-vortex flow, as seen in the figure, but how different this dependency is from 2D turbulence is also highlighted.

Figure 4(d-f) shows the PDF of  $\delta \equiv \text{Tr}(\mathbb{Z})$  for C particles. The  $\delta$  of individual particles was shifted in time by  $t_c$  before calculating the PDF. Fig. 4(h) shows  $\langle \delta \rangle$ , the mean of  $\delta$ , and the curves of different  $\alpha$  practically overlap. Around  $t = t_m$ ,  $\delta$  undergoes an inflection point. Beyond this, the magnitude decreases sharply, resulting in caustics at finite time. The maximum strain at  $t = t_m$  therefore triggers caustics at late times. This result, known for infinitely dense particles [18, 20, 44], also holds across density ratios, and underlines the importance of large strain regions in triggering caustics. An interesting final observation is that particles exit high-strain regions before  $t_c$  and caustics are actually formed in moderate strain regions. Thus, there is a universal mechanism of caustics formation across all density ratios.

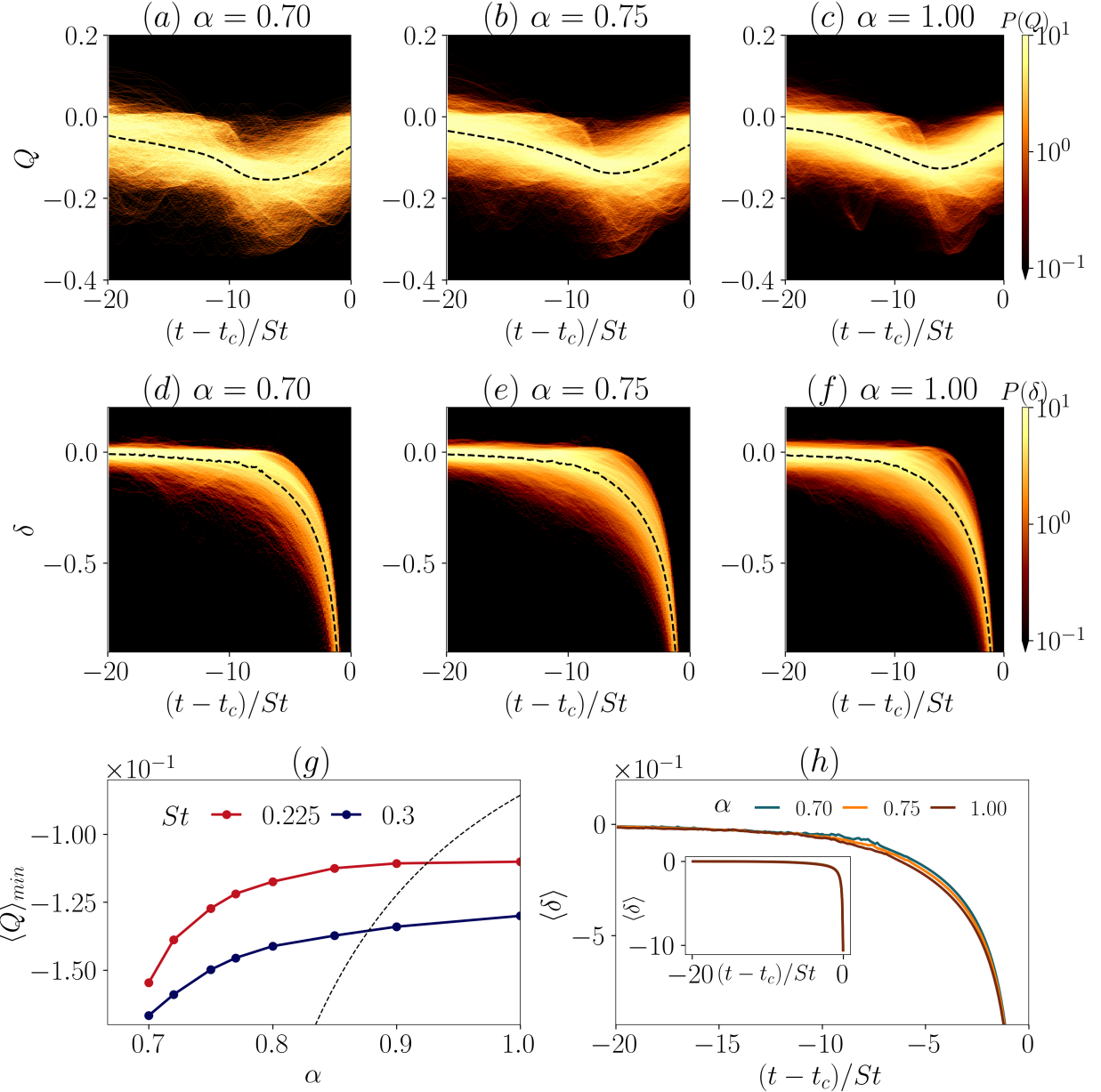


FIG. 4: (a-c) PDF of the  $Q$  explored by C particles of different density parameter  $\alpha$ . (d-f) the corresponding PDF of  $\delta = \text{Tr}(\mathbb{Z})$ . (g) Minimum of the average  $Q$  explored by particles on their way to caustics as a function of  $\alpha$ . (h) The mean of  $\delta$  shows similar behaviour across density ratios with an inflection to large negative values around the time of minimum  $Q$ .

## 2. Behavior of survivor S particles

Apart from the C and A particles seen before in point-vortex flows, another behavior is seen in turbulent flow, displayed by survivor or ‘S’ particles. These experience similar strain levels as the C particles, but never form caustics. We investigate them below.

Bätge *et al.* [20] found that not all infinitely-dense particles that visit regions of high strain form caustics. They derived a caustics criterion based on the eigenvalue magnitude of the fluid

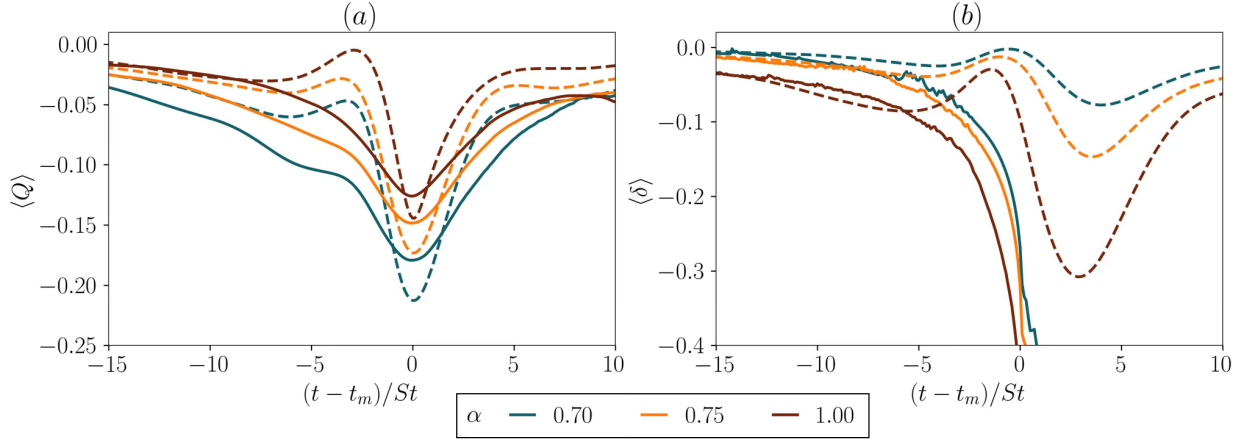


FIG. 5: Comparing (a)  $\langle Q \rangle$  and (b)  $\langle \delta \rangle$  of caustics C (solid lines) and survivor S (dashed lines) particles around the time they encounter a minimum in  $Q$ .

gradient and the time spent in large gradient regions. However, their analysis assumes that  $\mathbb{Z}$  and  $\mathbb{A}$  commute with each other, which is not true in general, due to the non-normality of  $\mathbb{A}$  [45]. A similar analysis for finitely-dense particles requires that in addition to  $\mathbb{A}$ ,  $D\mathbb{A}/Dt$  commute with  $\mathbb{Z}$  as well. This is not a fair assumption, and so a straightforward extension of [20] for finitely-dense particles is not possible. We show below that the time spent in strain regions is not the fundamental driver of the different dynamics of C and S particles. Rather, it is the time spent in extensional strain by the latter, which endows them with different pathline curvature and velocity, and the time spent in strain is a consequence of this.

To do this, we now shift the time of individual particles by their respective  $t_m$  and define  $Q_m$  as the mean of the minimum  $Q$  experienced by C particles. Note that the time-shift makes  $Q_m$  different from  $\langle Q \rangle_{min}$ . We define survivor S particles as those that sample  $Q \leq Q_m$ , but do not form caustics. The  $\langle Q \rangle$  as a function of the shifted time is shown in Fig. 5(a) for  $\alpha = 0.7, 0.75$  and  $1.0$ . After encountering the minimum all particles return to lower-strain regions. The broad trends are similar for C and S particles, but S particles explore larger negative  $Q$  regions — a consequence of our requirement that they visit a strain higher than  $Q_m$  — and also spend shorter times in them. We examine the differences in the history of C and S particles to explain the difference in their ultimate fate. One clue is obtained from Fig. 5(b), where we plot the mean of the  $\delta = \text{Tr}(\mathbb{Z})$  as a function of the shifted time  $(t - t_m)/St$ . Right before  $t = t_m$ , the  $\langle \delta \rangle$  of S particles rises to a maximum before plunging. This maximum is correlated with S particles visiting low-strain regions (see the maxima in Fig. 5(a)), which is not seen in the evolution of C particles. Thereafter S particles are subjected to a short duration of increasingly negative  $\langle \delta \rangle$  post  $t_m$ . And unlike C particles, their  $\delta$  recovers soon afterwards, and they avoid caustics. To explain the similarity in  $\langle Q \rangle$  and the dissimilarity in  $\langle \delta \rangle$  of C and S particles, we examine the strain and the vorticity of the background flow experienced by these particles, along with the curvature of the particle trajectories, and the alignment of the particle velocities with the local fluid strain directions. To do this, the velocity gradient tensor  $\mathbb{A}$  of the incompressible flow  $\mathbf{u}$  is written as

$$\mathbb{A} = St \begin{bmatrix} \sigma_n/2 & \sigma_s + \omega \\ \sigma_s - \omega & -\sigma_n/2 \end{bmatrix}, \quad (16)$$

where  $\sigma_n = \partial_x u_x - \partial_y u_y$ ,  $\sigma_s = \partial_x u_y + \partial_y u_x$ , are the normal and shear strains, respectively. The net strain given by  $\sigma = \sqrt{\sigma_s^2 + \sigma_n^2}$ . The eigenvalues of the strain tensor  $\mathbb{S} = (\mathbb{A} + \mathbb{A}^T)/2$  are  $\pm St \sigma/2$ ,

with the corresponding orthonormal eigenvectors

$$\hat{e}_\pm = \frac{1}{\sqrt{(\sigma_n \pm \sigma)^2 + \sigma_s^2}} (\sigma_n \pm \sigma, \sigma_s). \quad (17)$$

These eigenvectors  $\hat{e}_+$  and  $\hat{e}_-$  represent the extensional and the compressional directions of the local strain of the background fluid, respectively. A particle in a strain region where the background fluid velocity is aligned with  $\hat{e}_-$  experiences compressional strain, whereas one aligned with  $\hat{e}_+$  experiences extensional strain. In addition, if the particle's velocity is close to that of the background fluid, which is true for small Stokes particles, an alignment with  $\hat{e}_-$  represents the particle entering a saddle through compressional strain, and alignment with  $\hat{e}_+$  represents the particle exiting the saddle through extensional strain. The curvature of the particle's trajectory, defined as  $|\dot{\hat{v}}(t)/|\hat{v}(t)||$ , where  $\hat{v}$  is the unit vector of  $\hat{v}$ , indicates whether the particle is moving in a straight line, or along a curved or zigzag path. The degree of alignment of the particle velocity with the compressional or extensional direction of the strain is measured by the alignment angle  $\theta_v$ , given by

$$\sin \theta_v = \hat{v} \cdot \hat{e}_+, \quad \cos \theta_v = \hat{v} \cdot \hat{e}_-. \quad (18)$$

Thus,  $\theta_v = 0, \pi$  represents a particle moving along the compressional direction of the strain, whereas  $\theta_v = \pi/2, 3\pi/2$  indicates that the particle is moving along the extensional strain direction. For small Stokes particles,  $\theta_v = \pi/2$  and  $3\pi/2$  represent particles moving away from a local saddle point, whereas  $0$  and  $\pi$  represent motion towards it. Given the difference between these conditions, we do not expect complete top-down on left-right symmetry in any feature of  $\theta_v$ .

Fig. 6 highlights the differences between nearly-neutral C and S particles in terms of the metrics discussed above. Panel (a) shows the PDF of  $\theta_v$  at the times indicated in the  $\langle Q \rangle$  plot.  $\hat{e}_-(t)$  is calculated from Eq. (17) using the background strain at the location of the particle. Due to the small  $St$ ,  $\hat{v}$  and  $\hat{u}$  point in similar directions throughout. A stark difference between C and S particles is seen in the first panel, i.e., before the particles undergo sharply time-varying strains. With higher probability, C particles are better aligned with the compressional direction  $\hat{e}_-$ , whereas S particles preferentially orient along the extensional direction of strain  $\hat{e}_+$ , and experience a temporary reduction of strain, unlike C particles. Thereafter, both are catapulted into regions of high compressional strain (third panel) and finally (fourth panel) ejected into low-strain regions. The mean strain and vorticity magnitudes experienced by C and S particles are provided in Fig. 6 (b) and (c) for completeness. Important differences are evident in Fig. 6 (e) and (f) which show respectively that just prior to entering the maximum in strain (minimum in  $Q$ ), S particles move faster than C counterparts and that their paths have significantly less curvature. Due to shooting straight and rapidly through the high strain region, S particles spend less time there than C particles, and this is confirmed in the  $\langle Q \rangle$  plot in (a). The culmination of these differences is manifested in a dramatic departure in behaviour of C and S particles, as evidenced in Fig. 6 (d), where the former goes through caustics and the latter does not. Instead of a monotonic increase in negative  $\delta$ , S particles actually show a reduction, going briefly to almost no divergence.

Therefore, we conclude that encountering a compressive strain with a moderate particle velocity is critical in staying in large strain regions long enough to form caustics. On encountering extensive strain regions, particles dash out with significant velocity. Even if they encounter a compressive strain on their way out, their velocity is too high to stay in that compressive strain long enough to form caustics. Thus, apart from the strain magnitude, the nature of the strain encountered by the particles, compressive or extensive, is critical in forming caustics as it controls the time particles spend in large strain regions. This conclusion also holds across density ratios, and Fig. 7 shows similar behavior of infinitely dense  $\alpha = 1$  particles.

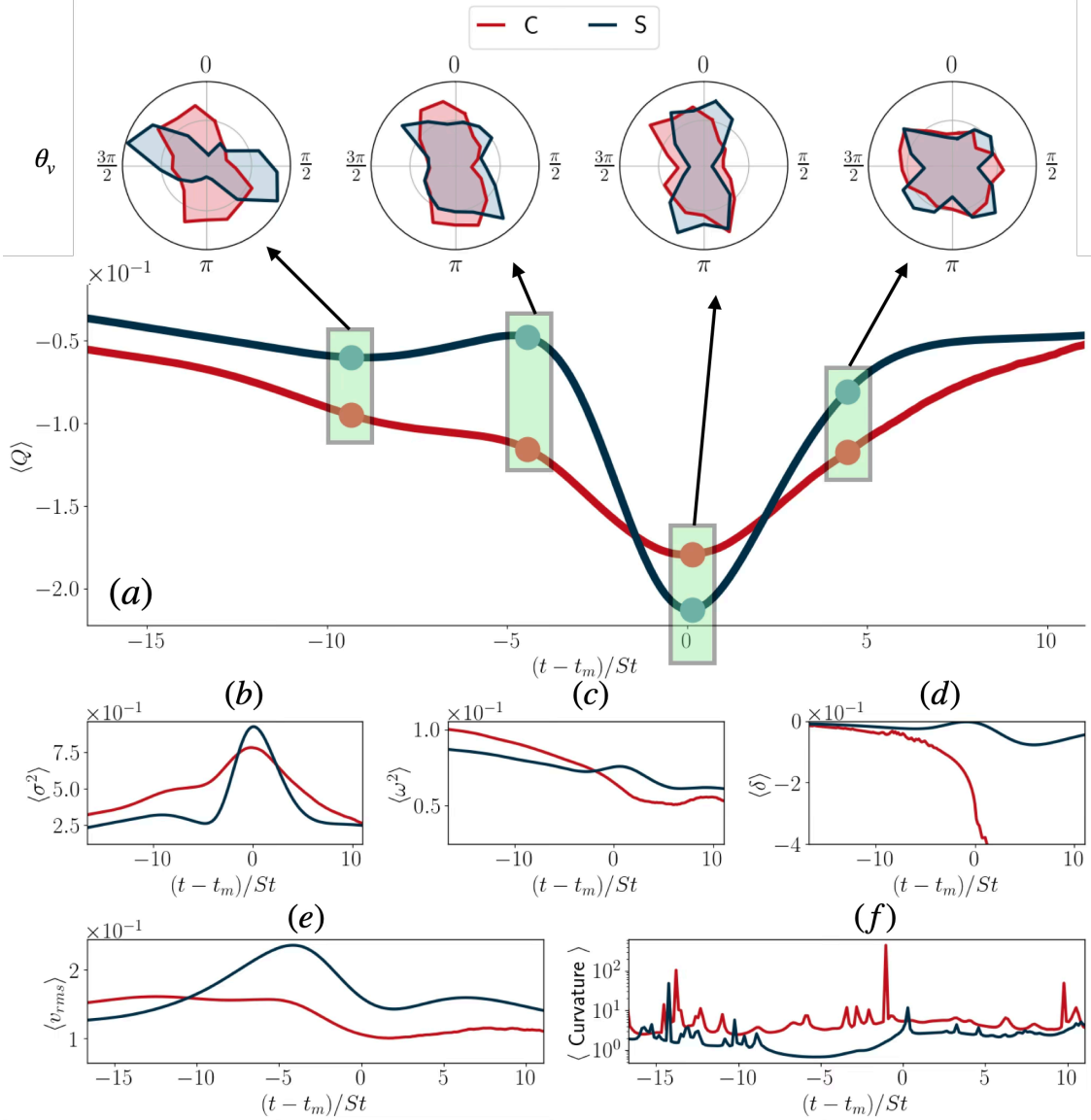


FIG. 6: Comparing  $\alpha = 0.7$  caustics and survivor particles using different metrics. Red is for C particles and blue for S ones. (a) PDFs of the alignment angle  $\theta_v$  are shown at times indicated by the green rectangles in the  $\langle Q \rangle$  plot. (b,c) Average strain and vorticity experienced by C and S particles during their evolution. (d) Average  $\delta = \text{Tr}(\mathbb{Z})$  for the C and S particles. Despite similar  $\langle Q \rangle$ s, their  $\langle \delta \rangle$  is significantly different. (e) RMS velocity of S particles is higher than the C particles, and their curvature (f) is much lower for some time before caustics.

Table I shows the relative numbers of particles in each category for different density ratios. Clearly, avoider A particles are in the majority, and for near-neutral particles, visiting high strain (C and S) is a rare event. A non-monotonicity is noticed in Fig. 8 in the relative fraction of C and S particles as  $\alpha$  increases. This is because of two factors. The sum of the two goes up with  $\alpha$  because the strain required is lower, as was seen in Fig. 4(g), and larger regions of the flow satisfy this. And at lower strain the propensity to go through extensional strain is lower, which makes survival difficult.

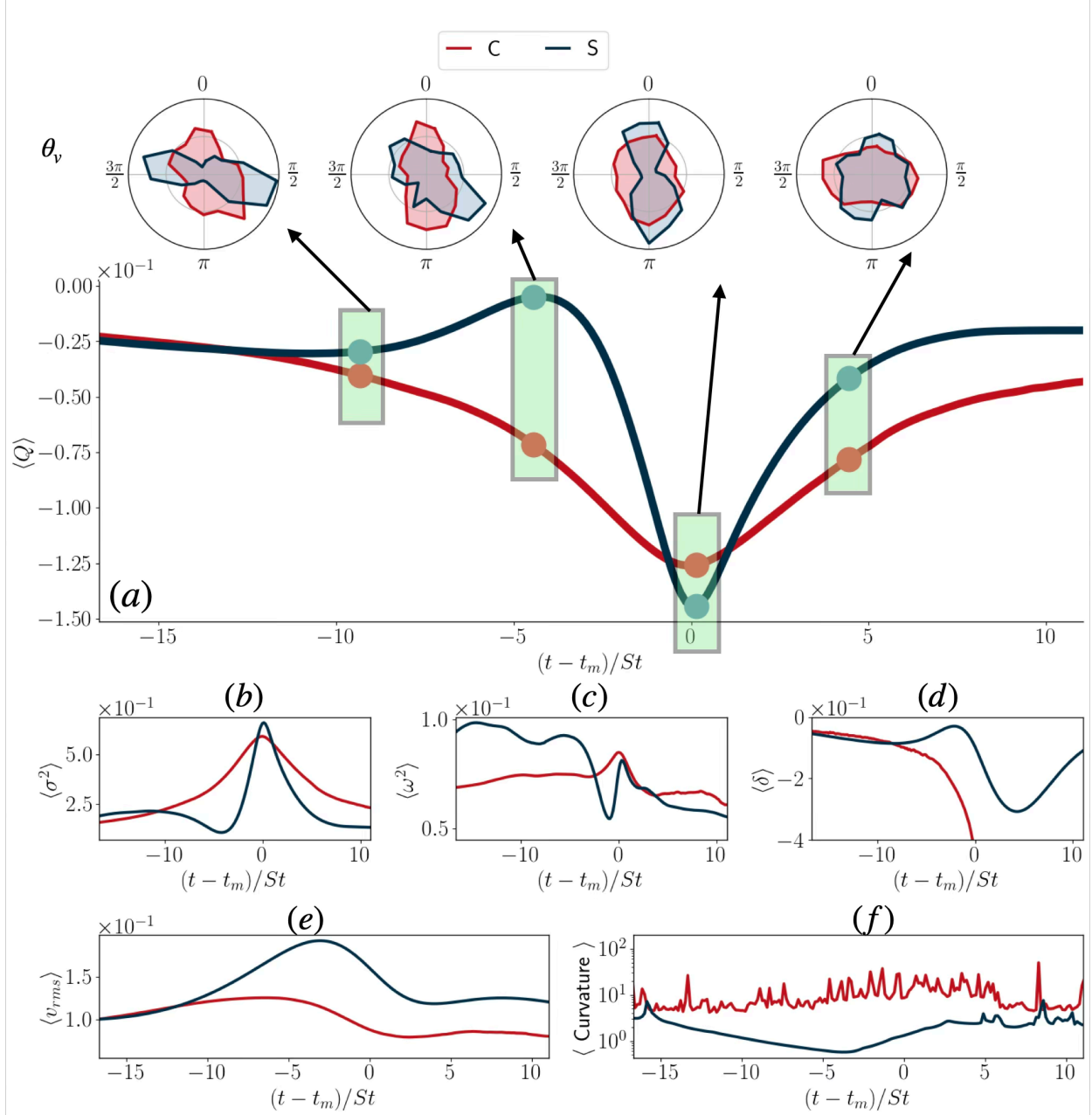


FIG. 7: Same as Fig. 6 but for infinitely dense  $\alpha = 1$  particles.

## V. CONCLUSION

To summarize, we investigate caustics formation — instances of extreme clustering — of finitely-dense spherical point-like particles one-way coupled to a background flow, and compare them to their better-studied infinitely-dense counterparts. We restrict ourselves to particles denser than the fluid. Added mass and the acceleration in the background flow affect caustics formation of finitely-dense particles.

We extend the caustics condition of Meibohm *et al.* [18] to the case of finitely dense frozen particles. The condition specifies regions of the background flow that can lead to caustics of particles

$\alpha$	Caustics	Survivors	Avoiders
0.70	0.0133	0.0662	0.9205
0.72	0.0306	0.1016	0.8678
0.75	0.0669	0.1233	0.8098
0.77	0.0906	0.1410	0.7684
0.80	0.1325	0.1431	0.7244
0.85	0.1970	0.1342	0.6688
0.90	0.2536	0.1193	0.6271
1.00	0.3099	0.1048	0.5854

TABLE I: Fraction of Caustics, Survivors, and Avoiders among 314000 particles at time  $t = 125\tau_\eta$  with  $St = 0.225$ .

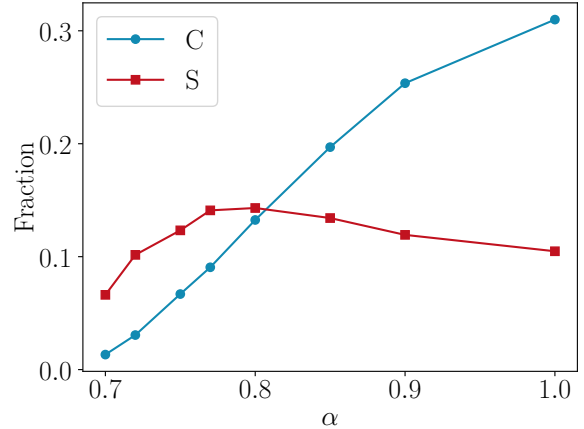


FIG. 8: Fractions of C and S particles at different density ratios.

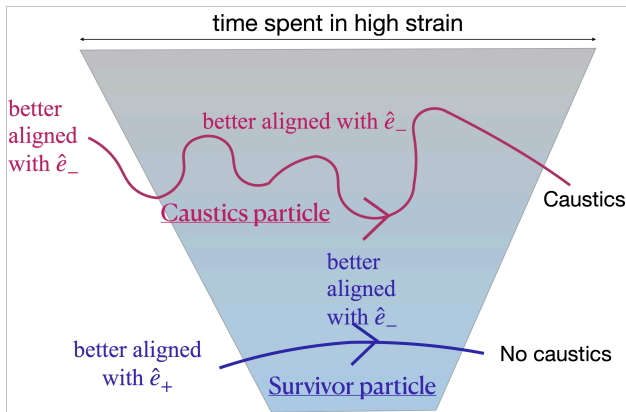


FIG. 9: Schematic of differences between C and S particles. The colored patch represents a region of high strain, and its horizontal extent the time spent by a particle within it. S particles pass quickly through this region and follow relatively straight paths, whereas C particles spend longer and adopt high-curvature paths. The early alignment with the extensive and compressive eigendirections of strain is the cause for these differences. At later times, both C and S particle-velocities are randomly oriented.

with vanishing Stokes number. It involves invariants of the fluid gradient tensor,  $Q$  and  $R$ , and the parameter  $\alpha$  that captures the density ratio.  $Q$  determines whether a region of the domain is vorticity dominated or strain dominated, while  $R$  compares the relative strength of vortex stretching and strain amplification. We find that the relation says that for finitely-dense particles heavier than the background flow, regions of large compressive strain, characterized by regions of negative  $Q$  and  $R$ , do not promote caustics. This contrasts with common intuition, where larger strain regions increase clustering of inertial particles denser than the fluid [2].

We investigate caustics in two scenarios: point vortex flow and 2D turbulence. Particles that originate below a critical density-dependent distance from a point vortex form caustics. Scaling the time with  $(3\alpha - 2)^{-1/2}$ , a data-collapse is obtained in the near-vortex region. As the particle becomes lighter, the caustics region shrinks, i.e., the strain levels required increase, and the time for caustics formation gets longer, so it is harder for lighter particles to form caustics. The frozen-particle

approach yielded a vastly different caustics region, and so, despite its analytical appeal, it is rather limited in reliability. Its predictions might hold for non-frozen particles with long residence times within the caustics region, but near a vortex, particles are typically centrifuged rapidly out of the vicinity.

In 2D turbulence too, only particles that go through high-strain regions can form caustics. As in point-vortex flow, caustics form after the particle has exited the high-strain region, and higher strain levels are needed for lighter particles. S particles go through high strain but do not form caustics, and our explanation for this, holding for particles of any density, is depicted in a schematic in Fig. 9. S particles first encounter a region of extensional strain. They eject out of these regions and into compressional strain regions along low curvature and high velocity paths, transiting quickly through the high-strain region without forming caustics. In contrast, C particles approach regions of large compressive strain with smaller velocity and large curvature, stay there for a significant time, and form caustics. Thus, our analysis not only explains the reason behind the Bätge *et al.* [20] findings for infinitely dense particles, but uncover the distinct history and mechanisms leading to the formation or the avoidance of caustics. In closing, we point out again that our findings are limited by our neglect of the Faxén and Basset-Boussinesq history forces on the particles. [32, 33] find that particle clustering for near-neutrally buoyant particles diminishes due to history forces at  $O(1)$  Stokes numbers, and we might expect a similar trend for caustics as well. Secondly, at higher  $St$  and lower  $\alpha$ ,  $Re_p$  may not remain small, and we need to obtain suitably modified particle dynamics. We believe our findings will apply in three-dimensional turbulence as well, but this is subject to confirmation by future studies. Additionally, non-spherical particles and higher number-densities that force the flow and each other need to be studied in the future, and we hope our work will motivate such studies.

## VI. ACKNOWLEDGEMENTS

We acknowledge support from the Department of Atomic Energy, Government of India, under project no. RTI4001. We thank Vijaykumar Krishnamurthy for access to GPU time. The final stages of the work were helped by the JC Bose Grant under the Anusandhan National Research Foundation of RG. Rajarshi thanks Divya Jagannathan, Saumav Kapoor, Tamoghna Ray, Jitendra Kethepalli, and Siddhartha Mukherjee for helpful discussions. We have no competing interests, and Microsoft and GitHub copilots were used for code development and plot formatting.

## VII. DATA AVAILABILITY

The code to run the simulations is publicly available on [GitHub](#). The data and scripts that can remake the plots are available on [Zenodo](#).

## Appendix A: Derivation of caustics condition for frozen caustics

To obtain Eq. (6), we extend the procedure outlined by [18] to the case of  $\alpha \neq 1$ . Defining the independent invariants of  $\mathbb{A}$  and  $\mathbb{Z}$  as

$$a = \text{Tr } \mathbb{A} = 0; \quad Q = -\frac{1}{2} \text{Tr } \mathbb{A}^2; \quad R = -\det \mathbb{A} = -\frac{1}{3} \text{Tr } \mathbb{A}^3; \quad z_2 = \text{Tr } \mathbb{Z}^2; \quad d = \det \mathbb{Z}, \quad (\text{A1})$$

we can write coupled algebraic equations for  $\delta, z_2, z_3$  in terms of  $Q$  and  $R$  by taking different powers of Eq. (7), taking their trace, and using Cayley-Hamilton theorem. Further, eliminating  $z_2$  and  $d$ ,

and defining  $\delta \equiv \pm\sqrt{\zeta} - 3\alpha/2$ , we get, after some algebra

$$\begin{aligned} & \left( \zeta^2 + \frac{a_2}{2}\zeta + a_0 \right)^2 + \zeta(a_1 - a_2a_0) = 0, \quad \text{where} \\ & a_0 = -\frac{3\alpha^4}{16} - (3\alpha + 1)\alpha^2Q + 36(\alpha - 1)\alpha R, \\ & a_1 = -\frac{7\alpha^6}{16} - 24(7 - 3\alpha)(1 - \alpha)\alpha^2Q^2 - \frac{1}{2}(21\alpha - 13)\alpha^4Q - 288(1 - \alpha)^2\alpha QR \\ & \quad - 1728(1 - \alpha)^3R^2 + 4(9\alpha + 7)\alpha^3R, \quad a_2 = 3[8(1 - \alpha)Q - \alpha^2]. \end{aligned} \quad (\text{A2})$$

The condition for caustics reduces to not having any positive root of  $\zeta$  in Eq. (A2). This happens when  $a_1 - a_2a_0 > 0$ , which yields Eq. (6).

- 
- [1] C. T. Crowe, R. A. Gore, and T. R. Troutt, Particle dispersion by coherent structures in free shear flow, *Particulate Science and Technology* **3**, 149 (1985).
- [2] E. Balkovsky, G. Falkovich, and A. Fouxon, Intermittent distribution of inertial particles in turbulent flows, *Physical Review Letters* **86**, 2790 (2001).
- [3] E. Calzavarini, M. Cencini, D. Lohse, and F. Toschi, Quantifying Turbulence-Induced Segregation of Inertial Particles, *Phys. Rev. Lett.* **101**, 084504 (2008).
- [4] G. Falkovich, A. Fouxon, and MG. Stepanov, Acceleration of rain initiation by cloud turbulence, *Nature* **419**, 151 (2002).
- [5] R. A. Shaw, Particle-turbulence interactions in atmospheric clouds, *Annual Review of Fluid Mechanics* **35**, 183 (2003).
- [6] M. Wilkinson, B. Mehlig, and V. Bezuglyy, Caustic activation of rain showers, *Physical review letters* **97**, 048501 (2006).
- [7] A. Pumir and M. Wilkinson, Collisional aggregation due to turbulence, *Annual Review of Condensed Matter Physics* **7**, 141 (2016).
- [8] C. Güttler, J. Blum, A. Zsom, C. W. Ormel, and C. P. Dullemond, The outcome of protoplanetary dust growth: Pebbles, boulders, or planetesimals?-I. Mapping the zoo of laboratory collision experiments, *Astronomy & Astrophysics* **513**, A56 (2010).
- [9] R. Schräpler and J. Blum, The physics of protoplanesimal dust agglomerates. VI. Erosion of large aggregates as a source of micrometer-sized particles, *The Astrophysical Journal* **734**, 108 (2011).
- [10] K. Wada, H. Tanaka, S. Okuzumi, H. Kobayashi, T. Suyama, H. Kimura, and T. Yamamoto, Growth efficiency of dust aggregates through collisions with high mass ratios, *Astronomy & Astrophysics* **559**, A62 (2013).
- [11] T. Birnstiel, Dust growth and evolution in protoplanetary disks, *Annual Review of Astronomy and Astrophysics* **62**, 10.1146/annurev-astro-071221-052705 (2024).
- [12] J. Meibohm, V. Pandey, A. Bhatnagar, K. Gustavsson, D. Mitra, P. Perlekar, and B. Mehlig, Paths to caustic formation in turbulent aerosols, *Physical Review Fluids* **6**, L062302 (2021).
- [13] G. Falkovich and A. Pumir, Sling effect in collisions of water droplets in turbulent clouds, *Journal of the Atmospheric Sciences* **64**, 4497 (2007).
- [14] A. Bhatnagar, V. Pandey, P. Perlekar, and D. Mitra, Rate of formation of caustics in heavy particles advected by turbulence, *Philosophical Transactions of the Royal Society A* **380**, 20210086 (2022).
- [15] R. Barta and J. Vollmer, Caustics in turbulent aerosols: An excitable system approach, *Journal of Fluid Mechanics* **949**, A36 (2022).
- [16] C. Meneveau, Lagrangian Dynamics and Models of the Velocity Gradient Tensor in Turbulent Flows, *Annu. Rev. Fluid Mech.* **43**, 219 (2011).
- [17] J. R. Picardo, L. Agasthya, R. Govindarajan, and S. S. Ray, Flow structures govern particle collisions in turbulence, *Physical Review Fluids* **4**, 032601 (2019).
- [18] J. Meibohm, K. Gustavsson, and B. Mehlig, Caustics in turbulent aerosols form along the Vieillefosse line at weak particle inertia, *Physical Review Fluids* **8**, 024305 (2023).

- [19] J. Meibohm, L. Sundberg, B. Mehlig, and K. Gustavsson, Caustic formation in a non-Gaussian model for turbulent aerosols, *Physical Review Fluids* **9**, 024302 (2024).
- [20] T. Bätge, I. Fouxon, and M. Wilczek, Quantitative prediction of sling events in turbulence at high Reynolds numbers, *Physical Review Letters* **131**, 054001 (2023).
- [21] M. R. Maxey and J. J. Riley, Equation of motion for a small rigid sphere in a nonuniform flow, *The Physics of Fluids* **26**, 883 (1983).
- [22] R. Gatignol, The faxén formulae for a rigid particle in an unsteady non-uniform stokes flow, (1983).
- [23] R. Volk, E. Calzavarini, G. Verhille, D. Lohse, N. Mordant, J.-F. Pinton, and F. Toschi, Acceleration of heavy and light particles in turbulence: Comparison between experiments and direct numerical simulations, *Physica D: Nonlinear Phenomena* **237**, 2084 (2008).
- [24] N. M. Qureshi, U. Arrieta, C. Baudet, A. Cartellier, Y. Gagne, and M. Bourgoin, Acceleration statistics of inertial particles in turbulent flow, *The European Physical Journal B* **66**, 531 (2008).
- [25] L. Fiabane, R. Zimmermann, R. Volk, J.-F. Pinton, and M. Bourgoin, Clustering of finite-size particles in turbulence, *Phys. Rev. E* **86**, 035301 (2012).
- [26] E. Karchniwy, A. Klimanek, and N. E. L. Haugen, The effect of turbulence on mass transfer rates between inertial polydisperse particles and fluid, *J. Fluid Mech.* **874**, 1147 (2019).
- [27] A. J. Petersen, L. Baker, and F. Coletti, Experimental study of inertial particles clustering and settling in homogeneous turbulence, *J. Fluid Mech.* **864**, 925 (2019).
- [28] Y. Motoori and S. Goto, Multiscale clustering of heavy and light small particles in turbulent channel flow at high Reynolds numbers, *International Journal of Heat and Fluid Flow* **102**, 109166 (2023).
- [29] E. Calzavarini, R. Volk, M. Bourgoin, E. Leveque, J.-F. Pinton, and F. Toschi, Acceleration statistics of finite-sized particles in turbulent flow: The role of Faxén forces, *Journal of Fluid Mechanics* **630**, 179 (2009).
- [30] V. Mathai, D. Lohse, and C. Sun, Bubbly and Buoyant Particle–Laden Turbulent Flows, *Annu. Rev. Condens. Matter Phys.* **11**, 529 (2020).
- [31] I. M. Mazzitelli, D. Lohse, and F. Toschi, The effect of microbubbles on developed turbulence, *Physics of Fluids* **15**, L5 (2003).
- [32] S. Olivieri, F. Picano, G. Sardina, D. Iudicone, and L. Brandt, The effect of the Basset history force on particle clustering in homogeneous and isotropic turbulence, *Physics of Fluids* **26**, 041704 (2014).
- [33] A. Daitche, On the role of the history force for inertial particles in turbulence, *J. Fluid Mech.* **782**, 567 (2015).
- [34] J. Ferry and S. Balachandar, A fast Eulerian method for disperse two-phase flow, *International journal of multiphase flow* **27**, 1199 (2001).
- [35] S. Kapoor, D. Jaganathan, and R. Govindarajan, Trapping and extreme clustering of finitely dense inertial particles near a rotating vortex pair, *Journal of Fluid Mechanics* **996**, A44 (2024).
- [36] M. S. Chong, A. E. Perry, and B. J. Cantwell, A general classification of three-dimensional flow fields, *Physics of Fluids A: Fluid Dynamics* **2**, 765 (1990).
- [37] S. Ravichandran and R. Govindarajan, Caustics and clustering in the vicinity of a vortex, *Physics of Fluids* **27**, 033305 (2015).
- [38] S. Ravichandran and R. Govindarajan, Waltz of tiny droplets and the flow they live in, *Physical Review Fluids* **7**, 110512 (2022).
- [39] Y. Ling, M. Parmar, and S. Balachandar, A scaling analysis of added-mass and history forces and their coupling in dispersed multiphase flows, *International Journal of Multiphase Flow* **57**, 102 (2013).
- [40] P. Deepu, S. Ravichandran, and R. Govindarajan, Caustics-induced coalescence of small droplets near a vortex, *Physical Review Fluids* **2**, 024305 (2017).
- [41] V. Pandey, P. Perlekar, and D. Mitra, Clustering and energy spectra in two-dimensional dusty gas turbulence, *Physical Review E* **100**, 013114 (2019).
- [42] M. A. T. van Hinsberg, J. H. M. Thije Boonkamp, F. Toschi, and H. J. H. Clercx, On the Efficiency and Accuracy of Interpolation Methods for Spectral Codes, *SIAM J. Sci. Comput.* **34**, B479 (2012).
- [43] E. Calzavarini, M. Kerscher, D. Lohse, and F. Toschi, Dimensionality and morphology of particle and bubble clusters in turbulent flow, *Journal of fluid mechanics* **607**, 13 (2008).
- [44] Y. Zhang and H. Xu, Caustics of inertial particles observed along Lagrangian particle trajectories, *Journal of Fluid Mechanics* **1014**, A13 (2025).
- [45] J. Kronborg and J. Hoffman, The triple decomposition of the velocity gradient tensor as a standardized real schur form, *Physics of Fluids* **35**, 031703 (2023).